Determination of Effective Mass for Continuous Contact Models in Multibody Dynamics

Parviz E. Nikravesh[1] . Mohammad Poursina [2]

Abstract

Continuous contact models have been popular in representing contact forces between impacting bodies of a multibody system. These models consider the contact force to be the result of a logical spring-damper element between the contacting bodies that exists for a very short period. The simplified and approximated model for generating the contact force is then assumed to be a mass-spring-damper system. Therefore, three common parameters that these models require are the spring stiffness, damping coefficient, and the so-called effective mass. For systems containing one degree-of-freedom, classical methods based on the kinetic energy have commonly been used to determine the effective mass. However, for multiple-degree-of-freedom multibody systems that contain kinematic joints, determination of the effective mass has not been adequately addressed in literature. This paper proposes a simple method for computing the effective mass based on the concept of impulse–momentum balance. This approach is applicable to both constrained and unconstrained equations of motion regardless of the multibody system's number of degrees-of-freedom.

Keywords *Effective mass . Apparent mass . Continuous contact . Impact*

1 Introduction

Collision between bodies could occur in some applications of multibody systems. To include a precise and accurate representation of impact or contact in the equations of motion of a system, we must consider the deformation, shape, and possibly other features of the contacting bodies [1]. In multibody dynamics, however, we need to combine all of these attributes into a very simple but relatively accurate approximate representation. For such a simplified representation, two different approaches are mostly considered. In one approach, known as the *piecewise* or *intermittent* analysis, it is assumed that the impact results in an instantaneous change in the velocities. A classical method to determine the change in the velocities considers balancing the system's momenta before and after an impact based on a given value for the *coefficient-of-restitution* [2, 3]. In the other approach, known as the *continuous* analysis, it is assumed that the impact causes contacting bodies to undergo local deformation in the contact region [4, 5].

[1] Parviz E. Nikravesh
Department of Aerospace and Mechanical Engineering, University of Arizona, Tucson, AZ, 85721, USA
E-mail: pen@arizona.edu

[2] Mohammad Poursina
Department of Engineering Sciences, University of Agder, Grimstad 4879, Norway
E-mail: poursina@uia.no

Either of the two methods is suitable for computational impact analysis in multibody dynamics. Both techniques require accurate determination of the exact time of contact. The continuous model also requires accurate determination of the exact time of loss of contact between impacting bodies. Since the piecewise approach assumes that the discontinuities in the velocities occur at an instant, its application is more feasible for impacts between bodies made of hard materials. For impacts between bodies with softer material, it is more common to apply the continuous method.

In the continuous model of impact, it is assumed that when two bodies collide, although the duration of contact is very small, the change in the velocities is not discontinuous. In other words, the velocities vary continuously during the period of contact as the contacting bodies undergo local deformations. The deformation is represented as a logical linear or nonlinear spring-damper element that applies a pair of resistive forces to the impacting bodies during the period of contact. As such, the simplified model for generating the contact force is assumed to be a mass-spring-damper system. The parameters of this equivalent system that need to be determined are effective mass, stiffness and damping coefficients, and the form of the nonlinearity.

In the past half-century, various models have been proposed that consider the force of the spring to be a nonlinear function of deformation, where stiffness of the spring could be determined based on the material and geometrical properties of the contacting regions [4-8]. The proposed models differ on whether the damping force, besides being a function of the deformation speed, should also be a function of the deformation itself or not. For these models, different formulas have been reported relating the damping coefficient to a desired value of the coefficient-of-restitution. Another parameter that needs to be determined for all of these models is the *effective mass*. For simple systems, in particular for systems containing only one degree-of-freedom, the effective mass can be determined using the kinetic energy of the bodies. However, for multibody systems containing kinematic joints or other constraints, and for systems having more than a single degree-of-freedom, determination of the effective mass becomes more complicated using the kinetic energy method.

In this paper a set of simple formulas for computing the effective mass is derived based on the concept of impulse–momentum balance. These formulas are applicable to both constrained and unconstrained equations of motion of multibody systems regardless of the system's number of degrees-of-freedom. However, before we discuss these formulas, a brief review of some of the proposed continuous contact models is provided. Finally, several examples are provided to clarify the use of the presented formulas in determining the effective mass.

2 Continuous contact models in direct central impact

In general, continuous contact models are developed based on the direct central impact between two spherical objects. In these models it is assumed that two spheres, having masses m_i and m_j, move with velocities v_i and v_j along an axis denoted by unit vector **n** normal to the tangent plane, as shown in Fig. 1(a) [9-14]. The local relative deformation is then viewed as an indentation (penetration) δ along the axis **n**. During the period of contact, these spheres continuously apply contact forces f_c and $-f_c$ on each other. The simplified and approximated model for generating the contact force is assumed to be a mass-spring-damper as depicted in Fig 1(b). In this scheme the contact cycle is divided into two phases: compression and restitution. The velocities of the colliding bodies just before impact at t^- are denoted as v_i^- and v_j^-. The compression phase starts at t^-, and then the indentation increases until it reaches a maximum value at which both spheres find the same velocity. At this moment the restitution phase begins which is followed by

a continuous decrease in the indentation until the spheres separate at ${}^{+}t$ with velocities ${}^{+}\boldsymbol{v}_i$ and ${}^{+}\boldsymbol{v}_j$.

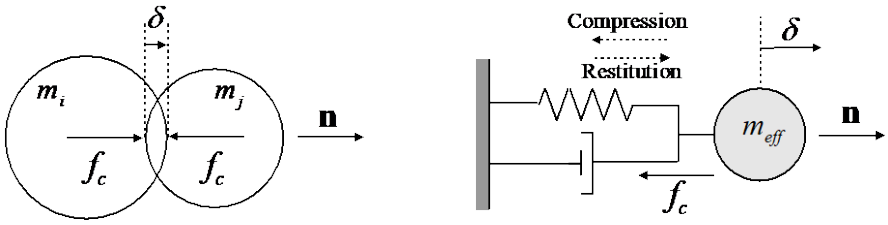

(a) (b)

Fig. 1 (a) Direct central impact of two spheres and (b) its equivalent continuous contact model representation

We can construct the equation of motion for each sphere during the contact along the axis **n** as $m_i\dot{v}_i = -f_c$ and $m_j\dot{v}_j = f_c$. Since in this one-dimensional system $\dot{\delta} = v_i - v_j$ and $\ddot{\delta} = \dot{v}_i - \dot{v}_j$, we can develop the following equation

$$m_{eff}\ddot{\delta} = -f_c \qquad (1)$$

where the *effective mass* is defined as

$$m_{eff} = \frac{m_i m_j}{m_i + m_j} \qquad (2)$$

Equation (1) represents the dynamics of the penetration with the following initial conditions:

$$\delta(0) = {}^{-}\delta = 0, \quad \dot{\delta}(0) = {}^{-}\dot{\delta} = {}^{-}v_i - {}^{-}v_j \qquad (3)$$

The main challenge in the continuous contact models is to determine a mathematical expression for f_c and tune its parameters based on known information about the system during the impact, while better capturing the physics of this phenomenon. Hertz model presents the contact force as a nonlinear spring [15]:

$$f_c = k\,\delta^n \qquad (4)$$

where *k* and *n* depend on the material properties and the local geometry of the contacting bodies. For two spheres in contact or for a locally spherical surface and a plane, for instance, $n = 3/2$, while for contacts between two locally plane surfaces $n = 1$ [16].

To consider energy dissipation during an impact, a linear damping force $c\dot{\delta}$ can be included, resulting in

$$f_c = c\dot{\delta} + k\,\delta^n \qquad (5)$$

With this description of the contact force, the dynamics of the penetration with the same initial conditions as in Eq. (3) can be expressed as

$$m_{eff}\ddot{\delta} + c\dot{\delta} + k\,\delta^n = 0 \qquad (6)$$

The behavior of this contact force model as a function of penetration is shown in Fig. 2(a). We observe that at initial contact time where $\delta = 0$ corresponding to point *A*, due to a nonzero relative initial velocity, there is a nonzero contact force. The penetration reaches its maximum value at *B* before the restitution phase begins. At point *C* the contact force reaches zero indicating that the bodies must separate even though the indentation has not reached zero. The dotted curve in this figure indicates that using this model beyond point *C* generates a nonphysical tensile force.

The use of the force model in Eq. (6), as of several decades ago, encountered difficulties due to computational limitations on both hardware and software. In forward dynamic integration of the equations of motion, it was not possible to predict the exact time of contact and separation at points *A* and *C*. However, today with the computational advancements of the past decades, the exact times of contact and separation can be determined accurately. Therefore, those computational limitations no longer exist.

However, another objection to the use of this model, based on experimental observations, has been the presence of the nonzero contact force at ^{-}t; i.e., point *A*.

To overcome the artifact of tensile force beyond point *C* and the nonzero contact force at point *A*, Hunt and Crossley [12] suggested the following contact force model that makes the damping force to be a function of both the indentation and its speed:

$$m_{eff}\ddot{\delta} + (\mu\dot{\delta} + k)\delta^{n} = 0 \quad (7)$$

where μ is called *hysteresis damping factor*. The behavior of this model is shown in Fig. 2(b) in solid curve, where for comparison purpose the behavior of the model in Eq. (6) is shown in dotted curve. We observe that the compression phase starts and the restitution phase ends at zero contact force and zero indentation. Although this model eliminates the undesirable tensile force after separation, some experimental observations indicate that the separation of the two bodies takes place before the indentation reaches zero [17].

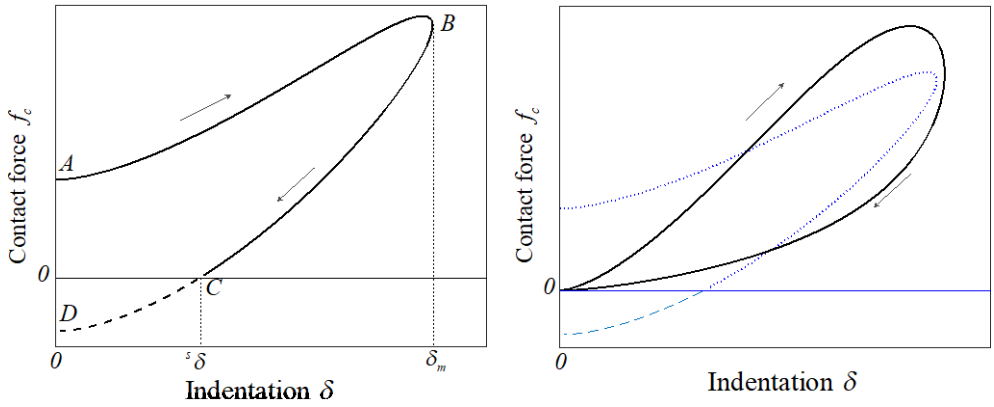

Fig. 2 Contact force versus indentation for (a) Eq. (6) and (b) Eq. (7)

3 Damping parameters and the coefficient of restitution

Whether we use the model of Eq. (6) or Eq. (7), the stiffness *k* is usually determined based on the material properties of contacting bodies and the geometry of contacting surfaces. However, the question that remains is how to determine the value of the damping coefficient *c* or the damping factor μ. Researchers have found it desirable to relate these damping parameters to the *coefficient-of-restitution* between the impacting bodies; i.e.,

$$e = -^{+}\dot{\delta} / ^{-}\dot{\delta} \quad (8)$$

For the model of Eq. (7) several formulas have been developed. Due to the locality of deformation during the period of contact, these formulas are derived mainly based on the local energy balance at the points of contact in a frictionless direct central impact. Lankarani et al. [16, 18], Hu et al. [11], Ye et al. [19] and Flores et al. [10] estimated the damping factor, respectively, as

$$\mu = \frac{3k(1-e^{2})}{4(^{-}\dot{\delta})} \quad (9)$$

$$\mu = \frac{3k(1-e)}{2e(^{-}\dot{\delta})} \quad (10)$$

$$\mu = \frac{8k(1-e)}{5e(^{-}\dot{\delta})} \quad (11)$$

The formula of Eq. (9) provides an acceptable estimate for the damping factor when the coefficient-of-restitution is close to one, where the models in Eqs. (10) and (11) can be used more accurately for the entire range of coefficient-of-restitution from zero to one.

Considering the fact that today the computational limitations of several decades ago are no longer issues, we can use the original contact model of Eq. (6), instead of Eq. (7), if this model better represents the behavior of our contact. Therefore, for this model we need to relate the damping coefficient c to other parameters in the model, specifically to the coefficient-of-restitution e.

For the commonly used value of $n = 3/2$, for two impacting spheres or a sphere and a plane, it has been shown through an optimization process that the damping coefficient in Eq. (6) can be computed as a function of other parameters as [20]

$$c = 1.95\ (e^{-0.3} - 1)\ k^{0.4}\ (\dot{\delta}^{-})^{0.2}\ m_{eff}^{0.6} \qquad (12)$$

A more general formula for any given value of n has also been reported for the damping coefficient, again through an optimization process, as [21]

$$c = \alpha\ (e^{\beta} - 1)\ [k\ (\dot{\delta}^{-})^{n-1}\ m^{n}]^{\frac{1}{n+1}} \qquad (13)$$

where

$$\alpha = 0.3331n^4 - 1.49n^3 + 3.077n^2 - 2.306n + 1.794$$

$$\beta = 1.285n^{0.2533} - 1.725$$

We can verify that for $n = 3/2$ Eq. (13) yields the same value for c as using Eq. (12).

4 Effective mass

For a continuous contact model, whether we use Eq. (6) or Eq. (7), we need to determine the effective mass between the two contacting bodies. As we have already seen, it is not difficult to determine the effective mass between two spherical objects in a direct central impact, as given in Eq. (2). Furthermore, for mechanical systems with one degree-of-freedom, the classical method of using kinetic energy can lead to correct determination of effective mass [22]. However, for systems with multiple degrees-of-freedom, this problem becomes more challenging even for two unconstrained bodies impacting each other; in particular, if the body mass centers, as shown in Fig. 3, do not lie on the axis of impact. The problem becomes even more complicated if the impacting bodies are part of a constrained multibody system since the instantaneous inertia of all the bodies, which are connected through kinematic joints, should contribute to the effective mass between the two impacting bodies.

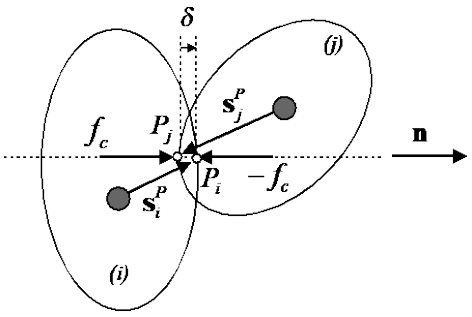

Fig. 3 Impact between two unconstrained bodies

In the past decades, several methods have been proposed to determine the effective mass in multibody systems when experiencing impact. Two such methods are namely the energy method and the Newtonian method. These two approaches consider the impact between bodies (i) and (j) of a multibody system as shown in Fig. 4(a). Both

techniques assume that body (*i*) is a member of subsystem-*i* and body (*j*) is a member of subsystem-*j*. The main objective is to model these two subsystems as two resulting spheres with *apparent* masses m_{app-i} and m_{app-j} as shown in Fig. 4(b). Then m_{app-i} and m_{app-j} are used in Eq. (2), instead of m_i and m_j, to find the effective mass at the point of contact between bodies (*i*) and (*j*). We could refer to m_{app-k}, for $k = i$ or j, as the apparent mass of subsystem-*k* or the apparent mass of body (*k*). (In references [13, 23, 24] the mass of a subsystem is referred to as "effective mass". However, in order not to confuse this mass with the effective mass that is used in Eq. (1), in this paper we use the term "apparent mass" instead of "effective mass" for a subsystem.)

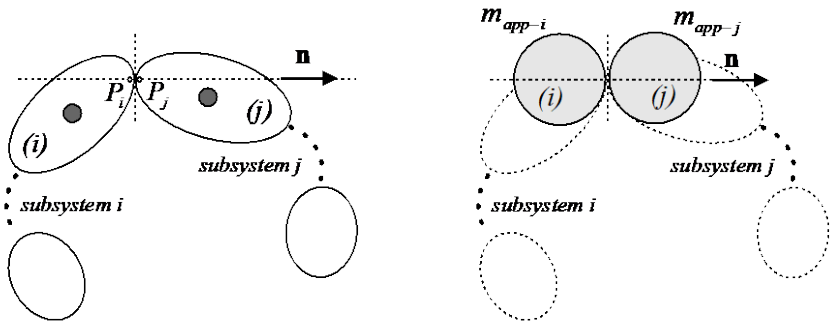

(a) (b)

Fig. 4 (a) Contact between bodies (*i*) and (*j*), each belonging to different subsystems. (b) Apparent masses of the subsystems are considered as the mass of two impacting spheres

The energy method assumes that the contribution of the kinematic joints between the bodies can be accounted for through the kinetic energy of the constituent subsystems [6]. This method works based on the hypothesis that kinetic energy of subsystem-*i* (or subsystem-*j*) can be given to a generalized mass m_{app-i} (or m_{app-j}) moving with the velocity which is the projection of the translational velocity of body (*i*) before the impact in the normal direction. Therefore, m_{app-i} and m_{app-j} are computed as

$$m_{app-k} = KE_{sub-k} \Big/ \tfrac{1}{2}(\mathbf{n}^{\mathrm{T}}\dot{\mathbf{r}}_k)^2 \text{ ; for } k = i, j \qquad (14)$$

In this equation, KE_{sub-k} is the kinetic energy of subsystem-*k* just before the impact, $\dot{\mathbf{r}}_k$ is the translational velocity of the mass center of body (*k*) right before the impact, $\mathbf{n}$ is the unit vector normal to the surface of contact, and the right-superscript T denotes vector (array or matrix) transpose. It should be noted that the velocities of the contact points projected on the normal direction might be different from those of the bodies. Additionally, the method does not consider the effect of rotation of the contacting bodies in the denominator of Eq. (14).

Similar to the previous approach, in the Newtonian method one finds m_{app-i} and m_{app-j} based on the dynamics of the subsystems they belong to. However, in this approach m_{app-k}, for $k = i, j$, is computed such that the inertial force acting on body (*k*) in the direction of $\mathbf{n}$ is equal to the inertial forces applied to the subsystem containing this body in the same direction, resulting in

$$m_{app-k} = \mathbf{n}^{\mathrm{T}} \sum_{s \in sub-k} m_s \ddot{\mathbf{r}}_s \Big/ \mathbf{n}^{\mathrm{T}} \ddot{\mathbf{r}}_k \text{ ; for } k = i, j \qquad (15)$$

In these equations, m_s denotes the mass of body (*s*), while $\ddot{\mathbf{r}}_s$ is the translational acceleration of the mass center of body (*s*) just before the impact [23, 24].

One of the challenges in these two approaches is the appropriate selection of subsystems when a multibody system contains multiple branches or closed chains. For instance, for the system shown in Fig. 5 where impacting bodies (*i*) and (*j*) are at the ends

of a kinematic chain and, therefore, it is not clear where to split the system to subsystem-*i* and subsystem-*j*. Another challenge of the energy method is that if the translational velocity of body (*i*) or body (*j*) in the contact normal direction right before impact becomes zero, the apparent mass of the corresponding subsystem becomes infinity. Similar challenge exists in the Newtonian Approach when the translational acceleration of one of the impacting bodies, in the contact normal direction, becomes zero the corresponding apparent mass becomes infinity. Finally, as stated in [23, 24], the apparent mass based on the energy method may not necessarily be the same as that of the Newtonian approach.

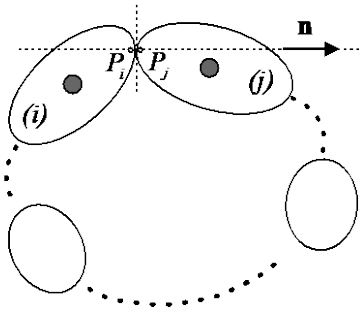

Fig. 5 Bodies (*i*) and (*j*) experience impact in a system containing a long kinematic chain

4.1 Impulse-momentum method to determine the effective mass

In this paper we propose an approach based on the impulse and the variation in relative velocity at the contact point in order to determine the effective mass between two impacting bodies. This technique does not suffer from the shortcomings of the approaches explained previously. For this purpose, we integrate Eq. (1) for the duration of contact:

$$m_{eff}\int_{^-t}^{^+t}\ddot{\delta}\,dt = -\int_{^-t}^{^+t} f_c\,dt \quad \Rightarrow \quad m_{eff}(^+\dot{\delta} - {}^-\dot{\delta}) = -\pi$$

where π denotes the impulse due to the contact force as a result of the impact. This equation can be simplified as

$$m_{eff} = \frac{\pi}{-\Delta\dot{\delta}} \qquad (16)$$

where $\Delta\dot{\delta} = {}^+\dot{\delta} - {}^-\dot{\delta}$. Note that the negative sign in Eq. (16) is due to the order of indices (*i*) and (*j*) that we have chosen in defining $\dot{\delta}$.

For a multibody system with n_b bodies, let us assume that bodies (*i*) and (*j*) in Fig. 3 impact each other at points P_i and P_j along the axis of the unit vector $\mathbf{n}$ normal to the tangent plane. We also assume that the contact between the two bodies lasts for a very short period of time, $\Delta t = {}^+t - {}^-t$, such that during impact the coordinates (positions and orientations) of the bodies do not change. We position the mass center of a typical body (*k*) with respect to an inertial reference frame by vector $\mathbf{r}_k$. Therefore, the translational velocity and acceleration vectors of the body are respectively denoted as $\dot{\mathbf{r}}_k$ and $\ddot{\mathbf{r}}_k$. Any desired set of rotational coordinates can be defined to describe the orientation of a body-fixed frame with respect to the inertial frame, with its origin at the body's mass center. Regardless of our choice for the rotational coordinates, the angular velocity and acceleration vectors of the body are respectively represented by vectors $\boldsymbol{\omega}_k$ and $\dot{\boldsymbol{\omega}}_k$. Therefore, 6×1 arrays of velocity and acceleration for this body are respectively defined as

$$\mathbf{v}_k = \begin{Bmatrix} \dot{\mathbf{r}}_k \\ \boldsymbol{\omega}_k \end{Bmatrix} \text{ and } \dot{\mathbf{v}}_k = \begin{Bmatrix} \ddot{\mathbf{r}}_k \\ \dot{\boldsymbol{\omega}}_k \end{Bmatrix}$$

We define an array of coordinates, $\mathbf{q}$, containing the translational and rotational coordinates of all the bodies, and two $6n_b \times 1$ arrays of velocities and accelerations, $\mathbf{v}$ and $\dot{\mathbf{v}}$, containing $\mathbf{v}_k$ and $\dot{\mathbf{v}}_k$ for $k = 1, \cdots, n_b$.

The kinematic joints in a multibody system yield kinematic constraints on the coordinates defined as nonlinear algebraic equations, $\boldsymbol{\Phi}(\mathbf{q}) = \mathbf{0}$. The time derivative of the constraints provides the velocity constraints that are linear in velocities and denoted as

$$\dot{\boldsymbol{\Phi}} = \mathbf{D}\,\mathbf{v} = \mathbf{0} \qquad (17)$$

where $\mathbf{D}$ is the *Jacobian* matrix of the kinematic constraints.

We construct the Newton-Euler equations of motion for each body; i.e., six equations per body. Then the equations of motion for the multibody system can then be represented in a general compact form as

$$\mathbf{M}\dot{\mathbf{v}} = \mathbf{g} + \mathbf{D}^{\mathrm{T}}\boldsymbol{\lambda} \quad (18)$$

where $\mathbf{M}$ is a $6n_b \times 6n_b$ inertia matrix, and $\mathbf{g}$ is a $6n_b \times 1$ array of applied loads as well as the gyroscopic terms for Euler's equations. The term $\mathbf{D}^{\mathrm{T}}\boldsymbol{\lambda}$ represents the array of reaction forces due to the kinematic joints, where $\boldsymbol{\lambda}$ is the array of Lagrange multipliers. For a system with n_{dof} degrees-of-freedom, there must be $n_c = 6n_b - n_{dof}$ independent constraints, which result in an $n_c \times 6n_b$ Jacobian $\mathbf{D}$ and n_c Lagrange multipliers.

For a system where bodies (i) and (j) impact each other at points P_i and P_j, the velocity of the contact points at any given time can be determined as

$$\dot{\mathbf{r}}_i^{P} = \dot{\mathbf{r}}_i - \tilde{\mathbf{s}}_i^{P}\boldsymbol{\omega}_i\,, \quad \dot{\mathbf{r}}_j^{P} = \dot{\mathbf{r}}_j - \tilde{\mathbf{s}}_j^{P}\boldsymbol{\omega}_j$$

where $\mathbf{s}_i^P$ and $\mathbf{s}_j^P$ are the position vectors of the contact points with respect to their corresponding body mass centers, as depicted in Fig. (3). Furthermore, the over-score tilde on a 3-vector transforms that vector to a 3×3 skew-symmetric matrix, meaning that $\tilde{\mathbf{s}}\boldsymbol{\omega}$ is the algebraic representation of the vector product $\vec{s} \times \vec{\omega}$. The relative velocity between the contact-points, following the same order of (i) and (j) as we used for two spheres, can be determined as

$$\begin{aligned}\dot{\mathbf{r}}_{ij}^{P} &= \dot{\mathbf{r}}_i^{P} - \dot{\mathbf{r}}_j^{P} = \dot{\mathbf{r}}_i - \tilde{\mathbf{s}}_i^{P}\boldsymbol{\omega}_i - \dot{\mathbf{r}}_j + \tilde{\mathbf{s}}_j^{P}\boldsymbol{\omega}_j \\ &= \begin{bmatrix} \mathbf{I} & -\tilde{\mathbf{s}}_i^{P} \end{bmatrix}\begin{Bmatrix} \dot{\mathbf{r}}_i \\ \boldsymbol{\omega}_i \end{Bmatrix} + \begin{bmatrix} -\mathbf{I} & \tilde{\mathbf{s}}_j^{P} \end{bmatrix}\begin{Bmatrix} \dot{\mathbf{r}}_j \\ \boldsymbol{\omega}_j \end{Bmatrix} = \begin{bmatrix} \mathbf{I} & -\tilde{\mathbf{s}}_i^{P} \end{bmatrix}\mathbf{v}_i + \begin{bmatrix} -\mathbf{I} & \tilde{\mathbf{s}}_j^{P} \end{bmatrix}\mathbf{v}_j\end{aligned}$$

where $\mathbf{I}$ is a 3×3 identity matrix. This equation can further be expressed in a compact form as

$$\dot{\mathbf{r}}_{ij}^{P} = \mathbf{D}_{ij}\,\mathbf{v} \qquad (19)$$

where

$$\mathbf{D}_{ij} = \left[\begin{array}{c|c|c|c|c} \mathbf{0}\cdots\mathbf{0} & \mathbf{I} \quad -\tilde{\mathbf{s}}_i^{P} & \mathbf{0}\cdots\mathbf{0} & -\mathbf{I} \quad \tilde{\mathbf{s}}_j^{P} & \mathbf{0}\cdots\mathbf{0} \end{array}\right] \quad (20)$$

is a $3\times6n_b$ matrix containing zero entries for all the bodies except for (i) and (j). The indentation speed between the contact points along the normal axis $\mathbf{n}$ can be determined as

$$\dot{\delta} = \mathbf{n}^{\mathrm{T}}\dot{\mathbf{r}}_{ij}^{P} = \mathbf{n}^{\mathrm{T}}\mathbf{D}_{ij}\,\mathbf{v} = \mathbf{d}_{ij}^{\mathrm{T}}\mathbf{v} \qquad (21)$$

where we have defined

$$\mathbf{d}_{ij} = \mathbf{D}_{ij}^{\mathrm{T}}\mathbf{n} \qquad (22)$$

Note that the array $\mathbf{d}_{ij}$ distributes a contact force along the axis $\mathbf{n}$ to the Newton's equations of motion and its corresponding moment to the Euler's equations on bodies (i) and (j).

As bodies (i) and (j) impact each other, a pair of impulsive contact forces of magnitude f_c acts at the contact points in opposite directions along the axis $\mathbf{n}$. The force $\mathbf{f}_c = \mathbf{n}f_c$ acts on body (j) resulting in a moment $\tilde{\mathbf{s}}_j^{P}\mathbf{f}_c$ about the mass center of body (j), and

the force $-\mathbf{f}_c = -\mathbf{n} f_c$ acts on body (*i*) resulting in a moment $-\tilde{\mathbf{s}}_i^P \mathbf{f}_c$ about the mass center of body (*i*). During the period of contact, these forces and the corresponding moments must be included in the equations of motion in an array $-\mathbf{D}_{ij}^{\mathrm{T}} \mathbf{f}_c = -\mathbf{D}_{ij}^{\mathrm{T}} \mathbf{n} f_c = -\mathbf{d}_{ij} f_c$. Therefore, Eq. (18) is revised to

$$\mathbf{M}\dot{\mathbf{v}} = \mathbf{g} + \mathbf{D}^{\mathrm{T}} \boldsymbol{\lambda} - \mathbf{d}_{ij} f_c \qquad (23)$$

If we integrate Eq. (23) for the period of contact $\Delta t = {}^{+}t - {}^{-}t$, and note that during this short period the coordinates, $\mathbf{M}$, $\mathbf{D}^{\mathrm{T}}$, $\mathbf{g}$, and $\mathbf{D}_{ij}^{\mathrm{T}}\mathbf{n}$ do not change, we then get

$$\mathbf{M}\int_{-t}^{-t} \dot{\mathbf{v}}\, dt = \mathbf{D}^{\mathrm{T}} \int_{-t}^{+t} \boldsymbol{\lambda}\, dt - \mathbf{d}_{ij} \int_{-t}^{+t} f_c\, dt$$

or

$$\mathbf{M}\,\Delta\mathbf{v} = \mathbf{D}^{\mathrm{T}} \Delta\boldsymbol{\sigma} - \pi\, \mathbf{d}_{ij} \qquad (24)$$

where $\Delta\mathbf{v} = {}^{+}\mathbf{v} - {}^{-}\mathbf{v}$, $\boldsymbol{\sigma} = \int \boldsymbol{\lambda}\, dt$, $\Delta\boldsymbol{\sigma} = {}^{+}\boldsymbol{\sigma} - {}^{-}\boldsymbol{\sigma}$, and $\pi = \int_{-t}^{+t} f_c\, dt$ is the impulse due to the contact.

Equation (21) can be revised for the change in the indentation speed along the normal axis before and after the impact as

$$\Delta\dot{\delta} = \mathbf{d}_{ij}^{\mathrm{T}} \Delta\mathbf{v} \qquad (25)$$

We note that Eqs. (24) and (25) contain the impulse π and $\Delta\dot{\delta}$, respectively.

4.2 Derivation with dependent coordinates

In the derivation leading to Eq. (24), the assumption was that there are n_c constraints due to the kinematic joints between the bodies, with the velocity constraints as expressed in Eq. (17). These velocity constraints must remain valid during the very short period of contact; i.e.,

$$\mathbf{D}\,\Delta\mathbf{v} = \mathbf{0} \qquad (26)$$

We append Eqs. (26) and (25) to Eq. (24) and arrange them in matrix form as

$$\begin{bmatrix} \mathbf{M} & -\mathbf{D}^{\mathrm{T}} & \mathbf{d}_{ij} \\ \mathbf{D} & \mathbf{0} & \mathbf{0} \\ \mathbf{d}_{ij}^{\mathrm{T}} & \mathbf{0} & 0 \end{bmatrix} \begin{Bmatrix} \Delta\mathbf{v} \\ \Delta\boldsymbol{\sigma} \\ \pi \end{Bmatrix} = \begin{Bmatrix} \mathbf{0} \\ \mathbf{0} \\ \Delta\dot{\delta} \end{Bmatrix} \qquad (27)$$

We define two scaled arrays $\Delta\mathbf{v}^{(s)} = \Delta\mathbf{v} / \Delta\dot{\delta}$ and $\Delta\boldsymbol{\sigma}^{(s)} = \Delta\boldsymbol{\sigma} / \Delta\dot{\delta}$, then using Eq. (16), Eq. (27) is expressed as

$$\begin{bmatrix} \mathbf{M} & -\mathbf{D}^{\mathrm{T}} & -\mathbf{d}_{ij} \\ \mathbf{D} & \mathbf{0} & \mathbf{0} \\ \mathbf{d}_{ij}^{\mathrm{T}} & \mathbf{0} & 0 \end{bmatrix} \begin{Bmatrix} \Delta\mathbf{v}^{(s)} \\ \Delta\boldsymbol{\sigma}^{(s)} \\ m_{\mathit{eff}} \end{Bmatrix} = \begin{Bmatrix} \mathbf{0} \\ \mathbf{0} \\ 1 \end{Bmatrix} \qquad (28)$$

This set of linear algebraic equations can be solved for the unknowns using any desired *efficient* numerical method; e.g., Gaussian elimination, where the solution directly yields the effective mass.

We can also derive a closed form expression for determining the effective mass. For this purpose, we rewrite Eq. (24) as

$$\Delta\mathbf{v} = \mathbf{M}^{-1}(\mathbf{D}^{\mathrm{T}} \Delta\boldsymbol{\sigma} - \pi\, \mathbf{d}_{ij})$$

We then substitute for $\Delta\mathbf{v}$ in Eqs. (25) and (26) to obtain

$$\mathbf{d}_{ij}^{\mathrm{T}} \mathbf{M}^{-1}(\mathbf{D}^{\mathrm{T}} \Delta\boldsymbol{\sigma} - \pi\, \mathbf{d}_{ij}) = \Delta\dot{\delta} \qquad (29)$$

$$\mathbf{D}\mathbf{M}^{-1}(\mathbf{D}^{\mathrm{T}} \Delta\boldsymbol{\sigma} - \pi\, \mathbf{d}_{ij}) = \mathbf{0} \qquad (30)$$

Equation (30) can be expressed as $\Delta\boldsymbol{\sigma} = \pi\left(\mathbf{D}\mathbf{M}^{-1}\mathbf{D}^{\mathrm{T}}\right)^{-1} \mathbf{D}\mathbf{M}^{-1}\mathbf{d}_{ij}$, which can then be substituted in Eq. (29), yielding

$$-\pi \mathbf{d}_{ij}^{\mathrm{T}} \mathbf{M}^{-1}\left(-\mathbf{D}^{\mathrm{T}}\left(\mathbf{D}\mathbf{M}^{-1}\mathbf{D}^{\mathrm{T}}\right)^{-1}\mathbf{D}\mathbf{M}^{-1}+\mathbf{I}\right)\mathbf{d}_{ij} = \Delta\dot{\delta}$$

Based on the definition in Eq. (16) we obtain the following:

$$m_{eff} = \frac{1}{\mathbf{d}_{ij}^{\mathrm{T}} \mathbf{M}^{-1}\left(-\mathbf{D}^{\mathrm{T}}\left(\mathbf{D}\mathbf{M}^{-1}\mathbf{D}^{\mathrm{T}}\right)^{-1}\mathbf{D}\mathbf{M}^{-1}+\mathbf{I}\right)\mathbf{d}_{ij}} \qquad (31)$$

This equation provides a closed-form formula for the effective mass between two impacting bodies of a constrained multibody system. The formula requires the inversion of two possibly large matrices, **M** and $\mathbf{D}\mathbf{M}^{-1}\mathbf{D}^{\mathrm{T}}$. The inertia matrix **M** in Newton-Euler equations of motion is a block-diagonal matrix, and its inverse can easily be determined in closed form. However, inverting matrix $\mathbf{D}\mathbf{M}^{-1}\mathbf{D}^{\mathrm{T}}$ could be numerically inefficient—this matrix is square and its dimensions depend on the number of kinematic constraints in the system. Therefore, it is computationally much more efficient to solve Eq. (28) instead of Eq. (31).

4.3 Derivation with independent coordinates

For a multibody system with n_{dof} degrees-of-freedom, we can define n_{dof} independent generalized coordinates, $\boldsymbol{\theta}$, and the corresponding independent generalized velocities $\dot{\boldsymbol{\theta}}$. Then, a velocity transformation matrix **B** can be constructed to provide the system velocity array **v** as [3]

$$\mathbf{v} = \mathbf{B}\dot{\boldsymbol{\theta}} \quad \Rightarrow \quad \Delta\mathbf{v} = \mathbf{B}\Delta\dot{\boldsymbol{\theta}} \qquad (32)$$

where **B** represents the null-space of the constraint Jacobian **D**; i.e., $\mathbf{D}\mathbf{B} = \mathbf{0}$. It should be noted that **B** does not change during the short period of contact as it only depends on the positions and orientations. Substituting Eq. (32) in Eq. (24) and pre-multiplying both sides by $\mathbf{B}^{\mathrm{T}}$ yield

$$\mathbf{M}_{dof}\,\Delta\dot{\boldsymbol{\theta}} = -\pi\,\mathbf{b}_{ij} \qquad (33)$$

where

$$\mathbf{M}_{dof} = \mathbf{B}^{\mathrm{T}}\mathbf{M}\mathbf{B} \qquad (34)$$

is the generalized $n_{dof} \times n_{dof}$ inertia matrix and

$$\mathbf{b}_{ij} = \mathbf{B}^{\mathrm{T}}\mathbf{D}_{ij}^{\mathrm{T}}\mathbf{n} = \mathbf{B}^{\mathrm{T}}\mathbf{d}_{ij} \qquad (35)$$

is an n_{dof} array. Substituting Eqs. (32) and (33) in Eq. (25) yields

$$\Delta\dot{\delta} = \mathbf{d}_{ij}^{\mathrm{T}}\,\mathbf{B}\,\Delta\dot{\boldsymbol{\theta}} = \mathbf{b}_{ij}^{\mathrm{T}}\,\Delta\dot{\boldsymbol{\theta}} \qquad (36)$$

We append Eq. (36) to Eq. (33) and rearrange the terms in matrix form, resulting in

$$\begin{bmatrix} \mathbf{M}_{dof} & \mathbf{b}_{ij} \\ \mathbf{b}_{ij}^{\mathrm{T}} & 0 \end{bmatrix} \begin{Bmatrix} \Delta\dot{\boldsymbol{\theta}} \\ \pi \end{Bmatrix} = \begin{Bmatrix} \mathbf{0} \\ \Delta\dot{\delta} \end{Bmatrix} \qquad (37)$$

Defining a scaled array of generalized velocities as $\Delta\dot{\boldsymbol{\theta}}^{(s)} = \Delta\dot{\boldsymbol{\theta}} / \Delta\dot{\delta}$ and using the definition of Eq. (16), we can express Eq. (37) as

$$\begin{bmatrix} \mathbf{M}_{dof} & -\mathbf{b}_{ij} \\ \mathbf{b}_{ij}^{\mathrm{T}} & 0 \end{bmatrix} \begin{Bmatrix} \Delta\dot{\boldsymbol{\theta}}^{(s)} \\ m_{eff} \end{Bmatrix} = \begin{Bmatrix} \mathbf{0} \\ 1 \end{Bmatrix} \qquad (38)$$

This small set of linear algebraic equations can be solved numerically to obtain the effective mass.

A closed form expression for the effective mass can easily be found from Eq. (38) as

$$m_{eff} = \frac{1}{\mathbf{b}_{ij}^{\mathrm{T}}\mathbf{M}_{dof}^{-1}\mathbf{b}_{ij}} \qquad (39)$$

We note that this equation has the same form as Eq. (31); however, it contains much smaller array and matrix. The inertia matrix $\mathbf{M}_{dof}$ is much smaller than the matrices in Eq. (31); therefore, computing its inverse is not numerically costly; e.g., for a system with one degree-of-freedom $\mathbf{M}_{dof}$ is a 1×1 matrix.

Referring to Eqs. (31) and (39), it is observed that the effective mass is independent of the velocities, accelerations, and the coefficient-of-restitution. This parameter is only a function of inertias, type of kinematic joints, and the topology of the system at the moment of impact.

5 Examples

Several simple examples are provided in this section to clarify the use of the formulas in Eqs. (28), (38), and (39). Although these formulas can easily be evaluated numerically, in some of these examples we determine the effective mass in closed-form in order to get a better insight to its meaning. Since these examples represent planar systems, we need to consider planar representation for all of our formulas. That is, if for a body in spatial formulations we have considered six coordinates (three translational and three rotational), for a body in planar motion we need to consider three coordinates (two translational and one rotational). Therefore, for example, for a system with n_b bodies in spatial motion we have $6n_b$ coordinates, where for the same system in planar motion we nave $3n_b$ coordinates, and so on. Detailed derivations for the equations of motion and constraints in planar multibody systems could be found in [3].

Example 1

This example considers a pendulum in planar motion impacting a wall as shown in Fig. 6. The main objective of this example is to provide a better understanding of what the *effective mass* is. Let us assume that the pendulum is a thin rod that is pinned to the ground at *O*. The length, mass, and polar moment of inertia of the rod are L, m, and $J = \frac{1}{12}mL^2$. It is further assumed that point *P* at the tip of the rod impacts a vertical wall represented by a unit vector **n** normal to its plane. Another unit vector **u** is defined perpendicular to the axis of the rod.

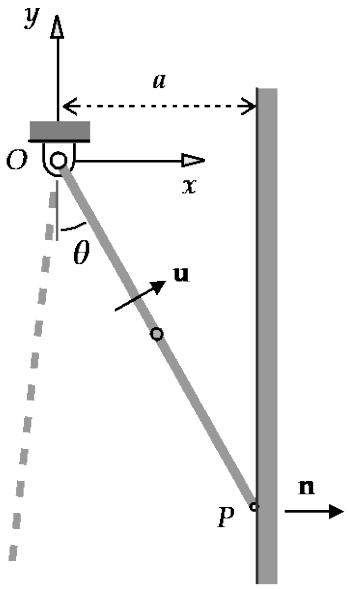

Fig. 6 A slender rod impacting a wall at its tip

Although we could apply any of the proposed formulas, since this is a single body with one degree-of-freedom, we apply Eq. (39) to determine the effective mass. We construct the following array and matrices:

$$\mathbf{n}=\left\{\begin{array}{c}\mathbf{1}\\ \mathbf{0}\end{array}\right\},\ \mathbf{D}_{ij}=\left[\begin{array}{cc}\mathbf{I} & \frac{1}{2}L\mathbf{u}\end{array}\right],\ \left\{\begin{array}{c}\dot{\mathbf{r}}\\ \dot{\theta}\end{array}\right\}=\left[\begin{array}{c}\frac{1}{2}L\mathbf{u}\\ \mathbf{1}\end{array}\right]\dot{\theta}\ \Rightarrow\ \mathbf{B}=\left[\begin{array}{c}\frac{1}{2}L\mathbf{u}\\ \mathbf{1}\end{array}\right],$$

$$\mathbf{M}=\left[\begin{array}{cc}m\mathbf{I} & \mathbf{0}_{2\times1}\\ \mathbf{0}_{1\times2} & \frac{1}{12}mL^2\end{array}\right]$$

where $\mathbf{I}$ represents a 2×2 identity matrix. We note that since this is a planar system, $\dot{\mathbf{r}}$ is a 2-vector and $\dot{\theta}$ is a single angular velocity. We find that $\mathbf{M}_{dof}=\mathbf{B}^{\mathrm{T}}\mathbf{M}\mathbf{B}=\frac{1}{3}mL^2$ and $\mathbf{b}_{ij}=\mathbf{B}^{\mathrm{T}}\mathbf{D}_{ij}^{\mathrm{T}}\mathbf{n}=L\mathbf{u}^{\mathrm{T}}\mathbf{n}=L\cos\theta$. Then Eq. (39) yields

$$m_{eff}=\frac{m}{3\cos^2\theta}\qquad(40)$$

We can verify Eq. (40) using the classical kinetic energy approach. Assuming that the pendulum has an angular velocity of $\dot{\theta}$, the velocity of point P becomes $\dot{\mathbf{r}}^{P}=L\dot{\theta}\mathbf{u}$, where its projection along the axis $\mathbf{n}$ is $\dot{\delta}=L\dot{\theta}\cos\theta$. We set the total kinetic energy of the pendulum equal to the kinetic energy of a particle at point P with a mass m_{eff} along the axis $\mathbf{n}$: $\frac{1}{2}(\frac{1}{3}mL^2)\dot{\theta}^2=\frac{1}{2}m_{eff}(L\dot{\theta}\cos\theta)^2$, which results in the same answer as in Eq. (40).

We now examine Eq. (40) for different values of the angle θ. For $\theta=0$, that is when $a=0$, Eq. (40) yields $m_{eff}=m/3$. As θ increases to 90 degrees, so does the value of the effective mass. At $a=L,\ \theta=90°$ results in $m_{eff}=\infty$. This means that no matter how large of a force we apply to the rod at point P along the rod's axis, due to the pin joint at O, the resulting acceleration along that axis will be zero. In other words, the rod (or point P) appears to have a mass of infinity.

Example 2

In this example we demonstrate the importance of the kinematic topology; i.e., the type and the orientation of the kinematic joints, in the determination of effective mass. This example consists of two spheres, bodies (*1*) and (*2*) as shown in Fig. 7, impacting each other in planar motion along an axis defined by unit vector $\mathbf{n}$ parallel to the x-axis. A third body is connected to body (*2*) by a frictionless sliding joint along an axis defined by unit vector $\mathbf{u}$ having an angle θ with respect to $\mathbf{n}$. The mass centers of all three bodies are on the x-axis during the collision. It is assumed that during impact no rotation is involved; therefore, we can only consider the translational equations of motion along the x- and y-axes.

In order to gain insight to the role of kinematic constraints in the evaluation of effective mass, we derive all the necessary arrays and matrices in closed form rather than numerically. If the mass centers are positioned from the origin of a nonmoving x-y plane by vectors $\mathbf{r}_i;\ i=1,2,3$, then the following velocity transformation can be constructed

$$\left\{\begin{array}{c}\dot{\mathbf{r}}_1\\ \dot{\mathbf{r}}_2\\ \dot{\mathbf{r}}_3\end{array}\right\}=\left[\begin{array}{ccc}\mathbf{I} & \mathbf{0}_{2\times2} & \mathbf{0}_{2\times1}\\ \mathbf{0}_{2\times2} & \mathbf{I} & \mathbf{0}_{2\times1}\\ \mathbf{0}_{2\times2} & \mathbf{I} & \mathbf{u}\end{array}\right]\left\{\begin{array}{c}\dot{\mathbf{r}}_1\\ \dot{\mathbf{r}}_2\\ \dot{d}\end{array}\right\}\ \Rightarrow\ \mathbf{B}=\left[\begin{array}{ccc}\mathbf{I} & \mathbf{0}_{2\times2} & \mathbf{0}_{2\times1}\\ \mathbf{0}_{2\times2} & \mathbf{I} & \mathbf{0}_{2\times1}\\ \mathbf{0}_{2\times2} & \mathbf{I} & \mathbf{u}\end{array}\right]$$

where in this planar example $\mathbf{I}$ represents a 2×2 identity matrix, and $\dot{d}$ is the relative velocity of the sliding block along the sliding axis with respect to body (*2*). The impact between the spheres occurs along the x-axis; i.e., along the unit vector $\mathbf{n}=\left\{\begin{array}{cc}1 & 0\end{array}\right\}^{\mathrm{T}}$. Matrix $\mathbf{D}_{ij}$ between bodies (*1*) and (*2*) and the mass matrix are constructed as

$$\mathbf{D}_{\ddot{i}\ddot{j}} = \begin{bmatrix} \mathbf{I} & -\mathbf{I} & \mathbf{0}_{2\times 1} \end{bmatrix}, \quad \mathbf{M} = \begin{bmatrix} m_1\mathbf{I} & & \\ & m_2\mathbf{I} & \\ & & m_3\mathbf{I} \end{bmatrix}$$

Then the array $\mathbf{b}_{\ddot{i}\ddot{j}}$ and the generalized mass matrix are found to be

$$\mathbf{b}_{\ddot{i}\ddot{j}} = \mathbf{B}^{\mathrm{T}}\mathbf{D}_{\ddot{i}\ddot{j}}^{\mathrm{T}}\mathbf{n} = \begin{Bmatrix} \mathbf{n} \\ -\mathbf{n} \\ 0 \end{Bmatrix}, \quad \mathbf{M}_{dof} = \begin{bmatrix} m_1\mathbf{I} & \mathbf{0}_{2\times 2} & \mathbf{0}_{2\times 1} \\ \mathbf{0}_{2\times 2} & (m_2+m_3)\mathbf{I} & m_3\mathbf{u} \\ \mathbf{0}_{1\times 2} & m_3\mathbf{u}^{\mathrm{T}} & m_3 \end{bmatrix}$$

We construct Eq. (38) as

$$\left[\begin{array}{ccc|c} m_1\mathbf{I} & \mathbf{0}_{2\times 2} & \mathbf{0}_{2\times 1} & -\mathbf{n} \\ \mathbf{0}_{2\times 2} & (m_2+m_3)\mathbf{I} & m_3\mathbf{u} & \mathbf{n} \\ \mathbf{0}_{1\times 2} & m_3\mathbf{u}^{\mathrm{T}} & m_3 & 0 \\ \hline \mathbf{n}^{\mathrm{T}} & -\mathbf{n}^{\mathrm{T}} & 0 & 0 \end{array}\right] \left\{\begin{array}{c} \Delta\bar{\mathbf{r}}_1^{(s)} \\ \Delta\bar{\mathbf{r}}_2^{(s)} \\ \Delta\bar{d}^{(s)} \\ m_{eff} \end{array}\right\} = \left\{\begin{array}{c} \mathbf{0}_{2\times 1} \\ \mathbf{0}_{2\times 1} \\ 0 \\ 1 \end{array}\right\}$$

where a numerical solution would provide us the value of the effective mass. However, since we are after a closed-form solution, we find the inverse of the generalized mass matrix to be

$$\mathbf{M}_{dof}^{-1} = \begin{bmatrix} \dfrac{1}{m_1}\mathbf{I} & \mathbf{0}_{2\times 2} & \mathbf{0}_{2\times 1} \\ \mathbf{0}_{2\times 2} & \dfrac{m_2\mathbf{I} + m_3\mathbf{u}\,\mathbf{u}^{\mathrm{T}}}{m_2(m_2+m_3)} & -\dfrac{\mathbf{u}}{m_2} \\ \mathbf{0}_{1\times 2} & -\dfrac{\mathbf{u}^{\mathrm{T}}}{m_2} & \dfrac{m_2+m_3}{m_2 m_3} \end{bmatrix}$$

Now we construct Eq. (39), and noting that $\mathbf{u}^{\mathrm{T}}\mathbf{n} = \cos\theta$, the effective mass is determined to be

$$m_{eff} = \frac{m_1 m_2 (m_2+m_3)}{m_2(m_2+m_3) + m_1(m_2 + m_3\cos^2\theta)} \quad (41)$$

Equation (41) clearly shows the dependence of the effective mass on the angle between the slider and the impact axes. We can examine this result for different values of the angle θ. For $\theta = 90°$, the effective mass is found to be $m_{eff} = \dfrac{m_1(m_2+m_3)}{m_1+(m_2+m_3)}$. In this configuration the axis of sliding is perpendicular to the axis of impact; therefore, bodies (*2*) and (*3*) appear as a single body with the apparent mass $m_2 + m_3$ impacting body (*1*). If we use the sum $m_2 + m_3$ as the mass of body (*2*) and m_1 for body (*1*) in the formula of Eq. (2), we obtain the same answer. For $\theta = 0°$, the effective mass is computed to be $m_{eff} = \dfrac{m_1 m_2}{m_1 + m_2}$. In this configuration the axis of sliding is parallel to the axis of impact; therefore, body (*3*) does not contribute to the mass of (*2*) and, therefore, to the effective mass.

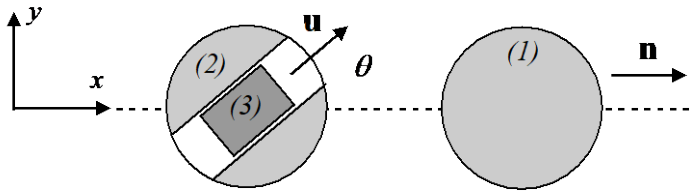

Fig. 7 Impact between two spheres where one contains a sliding mass

Example 3

The multibody system in this example, as shown in Fig. 8, is a planar system that contains a double pendulum, bodies *(1)* and *(2)*, and a single pendulum, body *(3)*. It is assumed that the tip of body *(2)*, point P_2, impacts body *(3)* at a point denoted as P_3. The link lengths and other necessary dimensions are given as $L_1 = 1.0$, $L_2 = 1.4$, $L_3 = 2.0$, and $a = 1.2$ (any desired units). The body mass centers are at the geometric centers G_i, $i =$ *1*,*2*,*3*. The mass of the bodies are $m_1 = 1.0$, $m_2 = 1.4$, and $m_3 = 2.0$. The moment of inertia of each link with respect to its mass center is evaluated as $J_i = \frac{1}{12} m_i L_i^2$, for $i =$ *1*,*2*,*3*. In the shown configuration when the impact occurs, the angle of the links with respect to the vertical axis are given as $\theta_1 = 30^o$, $\theta_2 = 60^o$, and $\theta_3 = 18.12^o$. In this configuration, the distance of the contact point P_3 from point *C* is found to be $d = 1.65$.

Since this is a simple system, we can easily construct Eq. (38) to find the effective mass. We choose the angles θ_1, θ_2, and θ_3 as three independent generalized coordinates. We construct three unit vectors perpendicular to each link as $\mathbf{u}_i = \left\{ \cos\theta_i \quad \sin\theta_i \right\}^{\mathrm{T}}$, for $i =$ *1*,*2*,*3*. We also note that the unit vector **n** along the impact axis is equal to $\mathbf{u}_3$.

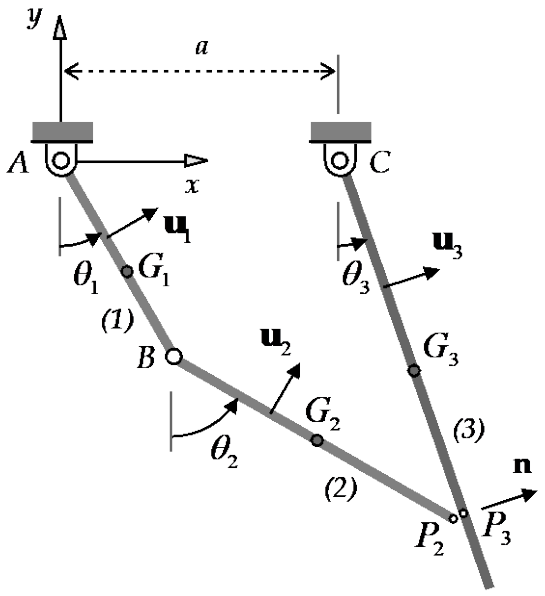

Fig. 8 A double pendulum impacting a single pendulum

We construct the generalized inertia matrix for the system, using any preferred method, as

$$\mathbf{M}_{dof} = \begin{bmatrix} (\frac{1}{3}m_1 + m_2)L_1^2 & \frac{1}{2}m_2 L_1 L_2 \cos(\theta_2 - \theta_1) & 0 \\ \frac{1}{2}m_2 L_1 L_2 \cos(\theta_2 - \theta_1) & \frac{1}{3}m_2 L_2^2 & 0 \\ 0 & 0 & \frac{1}{3}m_3 L_3^2 \end{bmatrix}$$

We can further generate matrix $\mathbf{b}_{\bar{ij}}$ directly by projecting the relative velocity between points P_2 and P_3 along the impact axis that is denoted by the unit vector **n** as

$$\mathbf{n}^{\mathrm{T}}(L_1\dot{\theta}_1\mathbf{u}_1 + L_2\dot{\theta}_2\mathbf{u}_2 - d\dot{\theta}_3\mathbf{u}_3) = \dot{\delta}$$

Or,

$$\begin{bmatrix} L_1\cos(\theta_1-\theta_3) & L_2\cos(\theta_2-\theta_3) & -d \end{bmatrix}\begin{Bmatrix} \dot{\theta}_1 \\ \dot{\theta}_2 \\ \dot{\theta}_3 \end{Bmatrix} = \dot{\delta}$$

where,

$$\mathbf{b}_{ij}^{\mathrm{T}} = \begin{bmatrix} L_1\cos(\theta_1-\theta_3) & L_2\cos(\theta_2-\theta_3) & -d \end{bmatrix}$$

Now we can construct and numerically solve Eq. (38) (or Eq. (39)) to find the effective mass to be $m_{eff} = 0.45$.

Example 4

In this example, we consider a slider-crank mechanism where the slider block impacts another sliding body as shown in Fig. 9. We assume the following data for this system (any consistent unit system): $L_1 = 1,\ L_3 = 2,\ m_1 = m_2 = m_4 = 1,\ m_3 = 2$, and $J_i = \frac{1}{12} m_i L_i^2$ for $i = 1,3$. It is assumed that when the crank angle is at 30 degrees, the slider block (*2*) impacts the slider (*4*).

To model this system, we define four generalized coordinates θ_1, x_2, θ_3, and x_4, in that order. It is determined that for $\theta_1 = 30^o$ we have $\theta_3 = 165.52^o$. Since the three coordinates that we have for the slider-crank are not independent, we have two loop-closure constraints. Therefore, we construct Eq. (28) to determine the effective mass.

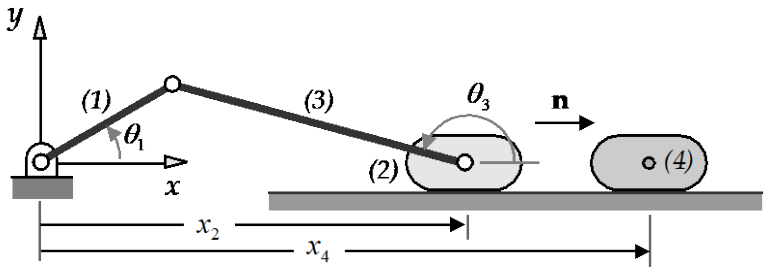

Fig. 9 The slider block, body (*2*), of this slider-crank mechanism impacts another slider block, body (*4*)

We determine the inertia matrix in closed form and also numerically to be

$$\mathbf{M} = \begin{bmatrix} \frac{1}{3}m_1L_1^2 & 0 & 0 & 0 \\ 0 & m_2+m_3 & -\frac{1}{2}m_3L_3\sin\theta_3 & 0 \\ 0 & -\frac{1}{2}m_3L_3\sin\theta_3 & \frac{1}{3}m_3L_3^2 & 0 \\ 0 & 0 & 0 & m_4 \end{bmatrix},\quad \mathbf{M} = \begin{bmatrix} 0.33 & 0 & 0 & 0 \\ 0 & 3.0 & -0.5 & 0 \\ 0 & -0.5 & 2.67 & 0 \\ 0 & 0 & 0 & 1 \end{bmatrix}$$

We find the Jacobian of the loop-closure constraints to be

$$\mathbf{D} = \begin{bmatrix} -L_1\sin\theta_1 & -1 & L_3\sin\theta_3 & 0 \\ L_1\cos\theta_1 & 0 & -L_3\cos\theta_3 & 0 \end{bmatrix},\quad \mathbf{D} = \begin{bmatrix} -0.5 & -1 & 0.5 & 0 \\ 0.87 & 0 & 1.94 & 0 \end{bmatrix}$$

Finally, the $\mathbf{d}_{ij}$ matrix is constructed as

$$\mathbf{d}_{ij}^{\mathrm{T}} = \begin{bmatrix} 0 & 1 & 0 & -1 \end{bmatrix}$$

Constructing Eq. (28) using these matrices, we compute the effective mass to be $m_{eff} = 0.8015$.

It would be an interesting observation to find out the apparent mass of subsystem-2, corresponding to body (*2*), since we know the effective mass and the mass of body (*4*). We substitute $m_4 = 1.0$ and $m_{eff} = 0.8015$ in Eq. (*2*) to determine m_{app-2}:

$$0.8015 = \frac{m_{app-2} \times 1.0}{m_{app-2} + 1.0} \quad \Rightarrow \quad m_{app-2} = 4.04$$

We note that the apparent mass of body (*2*) is much larger than its actual mass $m_2 = 1$. Now let us assume that the impact between the two sliders occurs when $\theta_1 = 0$; i.e., when the three bodies of the slider-crank are aligned along the *x*-axis. For this configuration if we solve Eq. (28), we find the effective mass to be $m_{eff} = 1.0$. Now if we determine the apparent mass of body (*2*) (using the similar approach explained previously), we find that $m_{app-2} = \infty$. This means that no matter how large of a force is applied on body (*2*), its acceleration remains zero, or as if its mass is infinity. Figure 10 shows the effective mass and the apparent mass of body (*2*) for the crank angle varying from zero to 90 degrees. We note that as the crank angle approaches zero the apparent mass of body (*2*) increases.

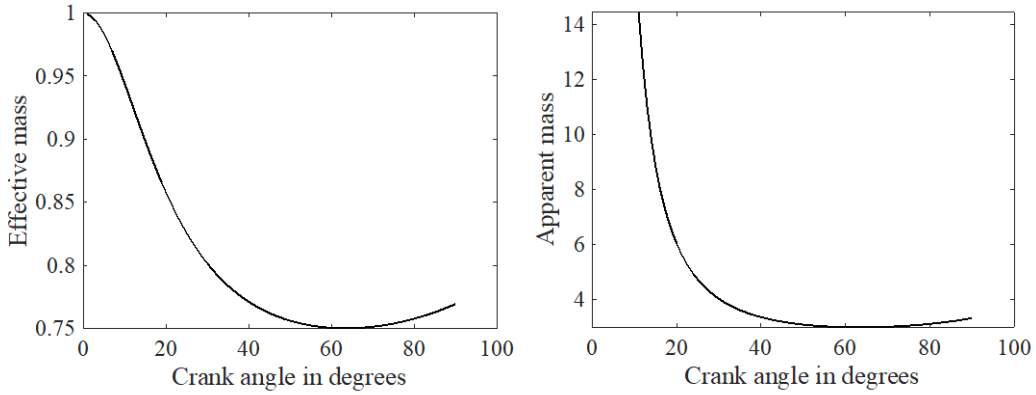

(a) (b)

Fig. 10 (a) Effective mass and (b) apparent mass of body (*2*) versus crank angle

Example 5

In this example we simulate the impact between two pendulums using three different contact models [21]. As shown in Fig. 11, the pendulums are modeled as slender rods with negligible thickness and uniform mass distribution. We assume following mass and geometric values: $m_1 = 1.0$, $m_2 = 0.2$ *kg*; $L_1 = 6.0$, $L_2 = 4.0$, $a = 2.0$ *m*. Each simulation starts with the configuration shown for the rods with solid boundaries, representing the initial conditions $\theta_1 = \pi/12$ *rad*, $\theta_2 = -\pi/2$ *rad*, and $\dot{\theta}_1 = \dot{\theta}_2 = 0$ *rad/s*. Other parameters that are considered in the models are: coefficient of restitution $e = 0.3$; Hertz contact parameters $n = 3/2$ and $k = 108$ $N/m^{1.5}$.

In the first simulation the piece-wise method based on the impulse-momentum formulation is used [3]. During the integration, as a contact is detected, the program halts the integration, determines the changes in the velocities based on the given coefficient of restitution, and then continues with the integration using the adjusted velocities. In the second simulation the Hunt-Crossley continuous contact model of Eq. (7) is considered. As a contact is detected, the program computes an updated damping factor using Eq. (11) based on the indentation speed between the contact points along the normal axis at the start of impact. Finally, in the third simulation the continuous contact force model of Eq. (12), which requires the determination of effective mass, is used to express the dynamics of impact during the period of contact. During the integration of the equations of motion, as a contact is detected, the effective mass is determined based on the instantaneous

values for the coordinates and velocities, and then the parameters for the contact force model are computed.

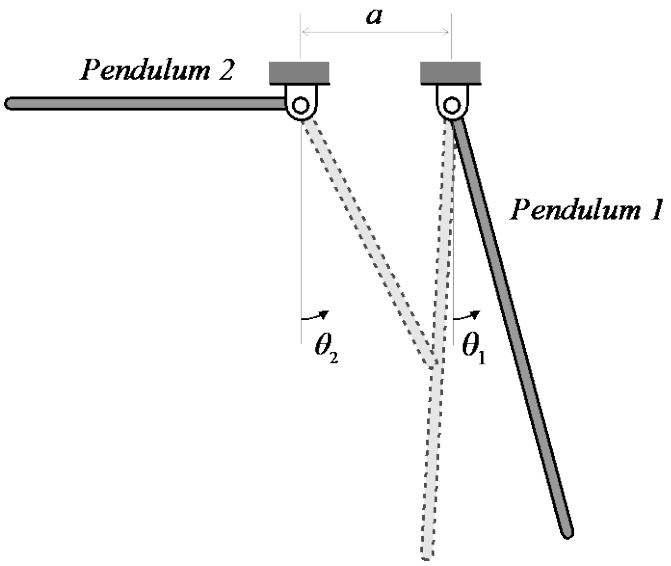

Fig. 11 Schematics of a two-pendulum system: the initial configuration of the system is shown by solid line and the configuration of the system at the first impact is shown by dotted line

Figure 12 shows the behavior of $\dot{\theta}_1$ and $\dot{\theta}_2$ for these simulations. It is observed that the system experiences three impacts during an 8-second simulation. The configuration of the system for the first impact is shown in Fig. 11 as dotted boundaries for the rods where $\theta_1 = -3^o$ and $\theta_2 = 27^o$. The results show that the response of the continuous contact force model of Eq. (12) is practically identical to that of the piece-wise method, where the response from the Hunt-Crossley force model begins to lag behind after each impact.

6 Conclusion

One of the common parameters in continuous contact models for multibody dynamics is the effective mass. For single-degree-of-freedom systems the classical method of using kinetic energy can determine the effective mass correctly. However, for systems with more than one degree-of-freedom the kinetic energy or other similar methods cannot provide a unique answer for the effective mass. The approach proposed in this paper, which is based on the concept of impulse–momentum balance, can uniquely determine this parameter regardless of the number of system's degrees-of-freedom. The method is applicable to both constrained and unconstrained equations of motion. The proposed concept shows that the effective mass is a function of the mass and rotational inertia of the bodies, the coordinates, and the type and orientation of the kinematic joints at the moment of impact.

The first formula that is derived in this paper for determining the effective mass considers the constrained Newton-Euler representation of the equations of motion. Then through a velocity transformation, the explicit presence of the kinematic constraints in the first formula is eliminated, yielding the second formula for determining the effective mass for unconstrained formulation. These formulas can be revised for any other representation of the constrained and unconstrained equations of motion for multibody systems.

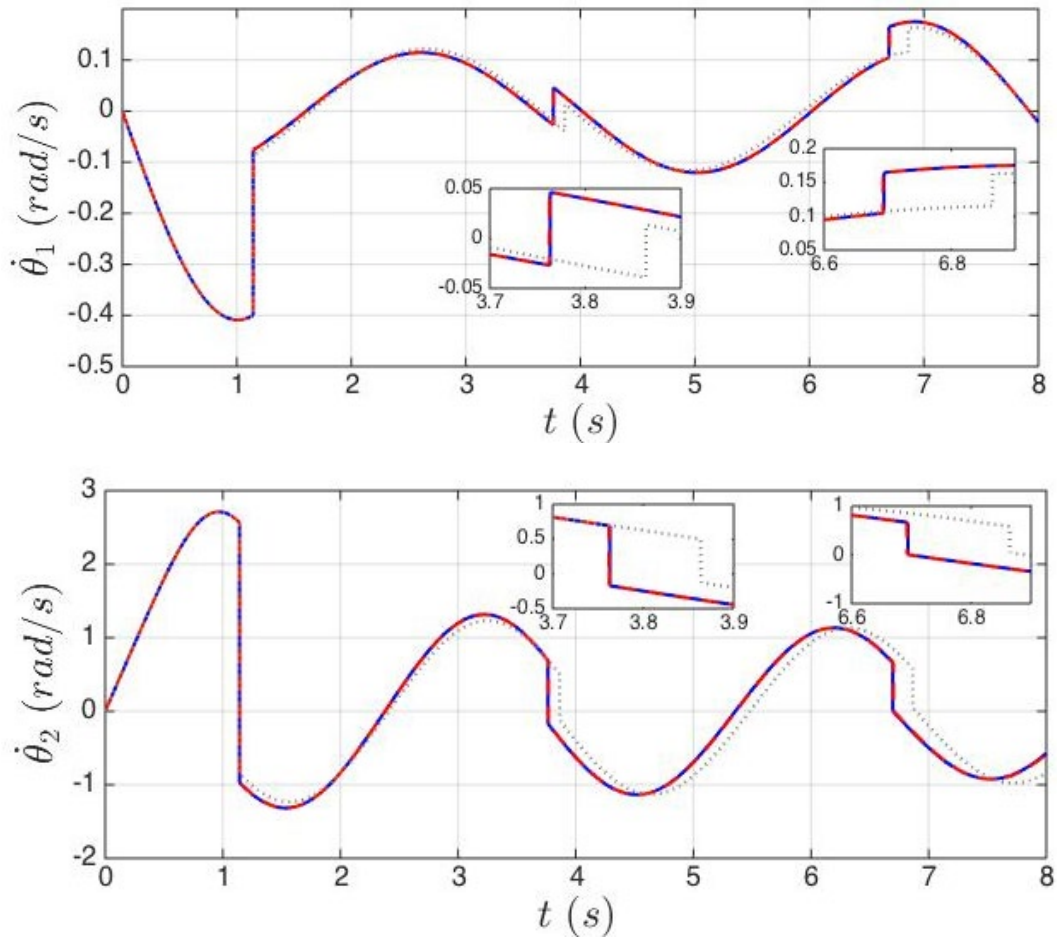

Fig. 12 Comparison between the results of the simulation of the double pendulum system, solid curve: piecewise method; dotted curve: Hunt and Crossley force model of Eq. (7); dashed curve: the continuous force model of Eq. (12)

7 Compliance with Ethical Standards

Funding: The authors did not receive support from any organization for the submitted work.
Financial interests: The authors have no relevant financial or non-financial interests to disclose.

8 References

1. Corral, E., Moreno, R. G., García, M. J. G., & Castejón, C.: Nonlinear phenomena of contact in multibody systems dynamics: A review. *Nonlinear Dyn.*, **104**(2), 1269-1295 (2021)
2. Mukherjee, R.M., Anderson, K.S.: Efficient methodology for multibody simulations with discontinuous changes in system definition. *Multibody Syst. Dyn.* **18**(2), 145–168 (2007)
3. Nikravesh, P.E.: Planar Multibody Dynamics: Formulation, Programming with MATLAB, and Applications, 2nd edn., CRC Press, Boca Raton (2018)
4. Carvalho, A. S., & Martins, J. M.: Exact restitution and generalizations for the Hunt-Crossley contact model. *Mech. Mach. Theory*, **139**, 174-194 (2019)

5. Machado, M., Moreira, P., Flores, P., & Lankarani, H. M.: Compliant contact force models in multibody dynamics: Evolution of the hertz contact theory. *Mech. Mach. Theory*, **53**, 99-121 (2012)
6. Wang, G., Liu, C., & Liu, Y.: Energy dissipation analysis for elastoplastic contact and dynamic dashpot models. *Int. J. Mech. Sci.* **221** (2022)
7. Jacobs, D. A., & Waldron, K. J.: Modeling inelastic collisions with the Hunt-Crossley model using the energetic coefficient of restitution. *J. Comput. Nonlinear Dyn.* **10**(2), 021001- 021010 (2015)
8. Rodrigues da Silva, M., Marques, F., Tavares da Silva, M., Flores, P.: A compendium of contact force models inspired by Hunt and Crossley's cornerstone work *Mech. Mach. Theory*, **167**, 104501-104520 (2022)
9. Anagnostopoulos, S.A.: Pounding of buildings in series during earthquakes. *Earthq. Eng. Struct. Dyn*. **16**(3), 443–456 (1988).
10. Flores, P., Machado, M., Silva, M.T., Martins, J.M.: On the continuous contact force models for soft materials in multibody dynamics. *Multibody Syst. Dyn*. **25**(3), 357–375 (2011). https://doi.org/ 10.1007/s11044-010-9237-4
11. Hu, S., Guo, X.: A dissipative contact force model for impact analysis in multibody dynamics. *Multibody Syst. Dyn*. **35**(2), 131–151 (2015) https://doi.org/10.1007/s11044-015-9453-z
12. Hunt, K., Crossley, F.R.E.: Coefficient of restitution interpreted as damping in vibroimpact. *J. Appl. Mech*. **42**(2), 440–445 (1975)
13. Khulief, Y.A., Shabana, A.A.: Dynamic analysis of constrained systems of rigid and flexible bodies with intermittent motion. *J. Mech. Transm. Autom. Des*. **108**, 38–45 (1986)
14. Lankarani, H.M., Nikravesh, P.E.: Hertz contact force model with permanent indentation in impact analysis of solids. In: 18th Annual ASME Design Automation Conference (1992). Publ. by ASME
15. Hertz, H.: *Gesammelte Werke*, vol. 1 (1895). Leipzig
16. Lankarani, H.M.: Canonical equations of motion and estimation of parameters in the analysis of impact problems. Ph.D. thesis, the University of Arizona (1988)
17. Wang, W., Hua, X., Wang X., Chen, Z., Song, G., J.: Advanced impact force model for low-speed pounding between viscoelastic materials and steel, Eng. Mech. (ASCE), **143**(12): 04017139 (2017)
18. Lankarani, H.M., Nikravesh, P.E.: Continuous contact force models for impact analysis in multibody systems. *Nonlinear Dyn.* **5**(2), 193–207 (1994) https://doi.org/10.1007/BF00045676
19. Ye, K., Li, L., Zhu, H.: A note on the hertz contact model with nonlinear damping for pounding simulation. *Earthq. Eng. Struct*. D **38**(9), 1135–1142 (2009) https://doi.org/10.1002/eqe.883
20. Poursina, M., Nikravesh, P.: Characterization of the damping coefficient in the continuous contact model. *J. Comput. Nonlinear Dyn.* **15**, (2020)
21. Poursina, M., Nikravesh, P.: Optimal damping coefficient for a class of continuous contact models, *Multibody Syst. Dyn*. **50**(2), 169-188 (2020) https://doi.org/10.1007/s11044-020-09745-x
22. Rao, S. S.: *Mechanical Vibrations*, *5th edn.*, Pearson (2010)
23. Lankarani, H.M., Ma, D., Menon, R.: Impact dynamics of multibody mechanical systems and application to crash responses of aircraft occupant/structure, *Computational Dynamics in Multibody Systems*, Pereira, M.F.O.S. and Ambrosio, J.A.C., eds., 239-265, Springer, Dordrecht, (1995)
24. Lankarani, H.M., Nikravesh, P.E.: "A contact force model with hysteresis damping for impact analysis of multibody systems," *ASME J. Mech. Design*, **112(**3), pp. 369-376 (1990)

(a) (b)
Fig. 1 (a) Direct central impact of two spheres and (b) its equivalent continuous contact model representation

(a) (b)
Fig. 2 Contact force versus indentation for (a) Eq. (6) and (b) Eq. (7)

Fig. 3 Impact between two unconstrained bodies

(a) (b)
Fig. 4 (a) Contact between bodies (*i*) and (*j*), each belonging to different subsystems. (b) Apparent masses of the subsystems are considered as the mass of two impacting spheres

Fig. 5 Bodies (*i*) and (*j*) experience impact in a system containing a long kinematic chain

Fig. 6 A slender rod impacting a wall at its tip

Fig. 7 Impact between two spheres where one contains a sliding mass

Fig. 8 A double pendulum impacting a single pendulum

Fig. 9 The slider block, body (*2*), of this slider-crank mechanism impacts another slider block, body (*4*)

(a) (b)
Fig. 10 (a) Effective mass and (b) apparent mass of body (*2*) versus crank angle

Fig. 11 Schematics of a two-pendulum system: the initial configuration of the system is shown by solid line and the configuration of the system at the first impact is shown by dotted line

Fig. 12 Comparison between the results of the simulation of the double pendulum system, solid curve: piecewise method; dotted curve: Hunt and Crossley force model of Eq. (7); dashed curve: the continuous force model of Eq. (12)